J Intell Robot Syst (2008) 53:119–143
DOI 10.1007/s10846-008-9234-5

Laser Pose Estimation and Tracking Using Fuzzy Extended Information Filtering for an Autonomous Mobile Robot

Hung-Hsing Lin · Ching-Chih Tsai

Received: 2 August 2007 / Accepted: 5 March 2008 /
Published online: 25 April 2008

Abstract This paper presents methodologies and techniques for posture estimation and tracking of an autonomous mobile robot (AMR) using a laser scanner with at least three retro-reflectors. A three-point laser triangulation method is presented to find an initial posture of the robot and then a fuzzy extended information filtering (FEIF) method is used to improve the accuracy of the robot's posture estimation. With the odometric information from the driving wheels, a FEIF-based posture tracking algorithm is proposed to continuously keep trace of the robot's posture at slow speeds. Simulation and experimental results are conducted to show the efficacy and usefulness of the proposed methods.

Keywords Extended information filtering (EIF) · Fuzzy logics · Laser scanner · Mobile robot · Self-localization · Posture tracking · Sensor fusion

1 Introduction

Posture estimation and tracking have become increasingly important and critical for autonomous mobile robots (AMRs) navigating in any flat environment. The robots with such self-localization capabilities are easy to achieve a free-ranging path tracking or a reactive navigation with a goal seeking behavior. In recent years, the laser technology has been considered as a powerful and accurate scheme for self-localization of the AMR. For navigation purpose, laser sensors can be divided into two technical categories: one is the scanning range-measuring time-of-flight laser; the other is an angle-measuring laser scanner with reflectors. Many studies have been done on applying laser range finders to solve for the robots' localization problems [6–9, 20]. Similarly, much attention has also been paid to the angle-measuring laser scanner [5, 13, 17] in both academia and industry. For instances, several international commercial companies, such as BT industries, have successfully

H.-H. Lin
Department of Electrical Engineering, Hsiuping Institute of Technology, Taichung 41280, Taiwan

C.-C. Tsai (✉)
Department of Electrical Engineering, National Chung Hsing University, Taichung 40227, Taiwan
e-mail: cctsai@dragon.nchu.edu.tw

produced angle-measuring laser-scanner-guided vehicles for industrial material handling in automatic factories.

The triangulation method for angle-measuring laser localization systems has been explored by several researchers [3, 11]. Toshihiro et al. [21] proposed an onboard angle-measuring laser localization system and the maximum likelihood estimation method to correct the estimated position of a mobile robot with the laser projector and the reflector. Tsumura et al. [19] proposed a 3-D position and attitude measurement system using laser scanners and corner cubes; in the system, each laser scanner rotated a fan-shaped laser beam for detecting the retro-reflections by the corner cubes and measures their azimuth angles. Rupp et al. [14] presented the optimized arrangement of artificial landmarks and then gave a solution for building an accurate and reliable localization system based on combining artificial and natural landmarks. Tsai et al. [17] developed and implemented using a complete and useful triangulation method an experimental angle-measuring laser scanning system; the main feature of their proposed method hinged on that both static position and orientation, termed the pose, of an AMR with respect to a reference frame can be determined uniquely by means of measuring the angles between the laser scanner and the retro-reflectors.

Although the extended Kalman filtering (EKF) method has already found extensive applications in robot navigation, it has been proven to have filter divergence problems due to noise variations or modeling errors. In order to deal with these disadvantages, the exponential data weighting method [12] was presented to improve the performance of this kind of filter by tuning both process and measurement noise covariance matrices. Abdelnour et al. [1] applied the fuzzy logics to on-line detection and correction of Kalman filter apparent and true divergence; they presented a fuzzy logic supervisor with three inputs, two outputs and 24 fuzzy rules. Other approaches of using fuzzy logics to adapt the Kalman filter for sensor fusion applications have been documented in [6, 9, 10, 15, 16]. On the other hand, the information form of the Kalman filter was well discussed in [12], who recently employed information estimation as a principal filtering technique. Although the information filter is algebraically equivalent to the Kalman filter, the former has been shown to possess advantages, such as low computational complexity, ease of initialization and decentralization, over the latter in multi-sensor data fusion applications. However, like EKF, the extended information filtering (EIF) method is still subjected to filter divergence problems due to noise variations or modeling errors. To prevent the EIF from divergence, the authors in [18] proposed a fuzzy extended information filter (FEIF) which consists of a fuzzy tuner to automatically adjust its exponential weightings for both process and measurement noise covariance matrices. Chang et al. [4] applied a fuzzy extended information filter to address the posture tracking problem of a mobile robot with the angle-measuring laser scanner; however, their proposed method was impractical because several bearing measurements were assumed to obtain simultaneously.

The paper is written with two principal objectives. The first one is to apply the fuzzy extended information filter (FEIF) in [18] to improve the accuracy of the static posture estimation or posture initialization for the AMR with an experimental angle-measuring laser scanner. With the same filtering approach, the second one is to find the optimal position and orientation estimates of the AMR using the dead-reckoning information and only one angle reflector measurement; this technique is proposed to not only circumvent the difficulty encountered in [4], but also improve the accuracy and robustness of the moving vehicle's position and orientation estimates under system modeling errors or measurement noise processes with variable covariance matrices.

The remainder of the paper is outlined as follows. Section 2 briefly introduces the fuzzy extended information filtering method. Section 3 describes the laser triangulation method

and the static posture estimation for initializing or localizing the mobile robot. In Section 4, we show how to apply the fuzzy extended information filtering to achieve robot pose tracking. Computer simulations and experimental results are conducted in Section 5 to verify the efficacy of the proposed posture estimation and tracking algorithms. Section 6 concludes this paper.

2 Fuzzy Extended Information Filtering

This section is dedicated to elucidating the fuzzy extended information filtering method. Consider the following nonlinear discrete-time system model and measurement model as follows:

$$X(k+1) = f(X(k), U(k), k) + W(k) \tag{1}$$

$$Z(k) = h(X(k), k) + V(k) \tag{2}$$

where $f(\cdot)$ and $h(\cdot)$ are nonlinear functions of the state $X(k)$ and the input $U(k)$, and twice differentiable. The vectors, $W(k)$~$N(0,Q(k))$ and $V(k)$~$N(0,R(k))$ are the associated process noise and the measurement noise, respectively. In order to obtain the best posture estimation and tracking of the mobile robot, the fuzzy extended information filtering algorithm is briefly stated as follows.

2.1 Exponential Weighted Extended Information Filter

The essential part of the fuzzy extended information filter (FEIF) is that this filter consists of a fuzzy tuner to automatically adjust its exponential weightings for both process and measurement noise covariance matrices. Given the state Eq. 1 and the measurement Eq. 2, we assume that the process and measurement noise covariance matrices are described by

$$R(k) = R \cdot \alpha^{-\beta(k+1)} \tag{3}$$

$$Q(k) = Q \cdot \alpha^{-\beta(k+1)} \tag{4}$$

where α is the weighting factor near one, β is the variation of exponential function, and constant matrices R and Q are with right dimensions. Given an initial state estimate $\widehat{X}(0/0)$, an initial information state $y_\alpha(0/0)$, and an initial information matrix $Y_\alpha(0/0)$, the well-known exponential weighted EIF whose prediction and estimation equations can be easily derived as follows:

(1) One-step-ahead Prediction

$$\widehat{y}_\alpha(k|k-1) = Y_\alpha(k|k-1) \times f\left(\widehat{X}(k-1|k-1), U(k-1), (k-1)\right) \tag{5}$$

$$Y_\alpha(k|k-1) = \left[\alpha^\beta \nabla f_X(k-1) Y_\alpha^{-1}(k-1|k-1) \times \nabla f_X^T(k-1) + Q\right]^{-1} \tag{6}$$

(2) Estimation (Measurement Update)

$$\widehat{y}_\alpha(k|k) = \widehat{y}_\alpha(k|k-1) + \nabla h_X^T(k)\left(\frac{R}{\alpha^\beta}\right)^{-1} \times \left[r(k) + \nabla h_X(k)\widehat{X}(k|k-1)\right] \tag{7}$$

$$Y_\alpha(k|k) = Y_\alpha(k|k-1) + \nabla h_X^T(k)\left(\frac{R}{\alpha^\beta}\right)^{-1} \nabla h_X(k) \tag{8}$$

where

$$r(k) = Z(k) - h\left(\widehat{X}(k|k-1)\right) \tag{9}$$

$$\nabla f_X(k-1) = \left.\frac{\partial f}{\partial X}\right|_{X=\widehat{X}(k-1|k-1)}, \ \nabla h_X(k) = \left.\frac{\partial h}{\partial X}\right|_{X=\widehat{X}(k|k-1)}.$$

Note that if α=1, then this filter becomes a regular EIF.

2.2 Fuzzy Tuner

The proposed fuzzy tuner is employed to monitor the innovations, to avoid divergence of the EIF and to tune the value of α in Eqs. 7–9. There are three inputs and one output designed for the fuzzy tuner. The mean value, the second-order moment and moment slew rate of the innovations are considered as the inputs to monitor the degree of filter divergence. By selecting certain sample number l, the three inputs of the fuzzy tuner are given as follows;

1. Statistical mean of the innovations:

$$\overline{r} \cong \frac{1}{l}\sum_{k=1}^{l} r(k) \tag{10}$$

2. Statistical second-order moment of the innovations:

$$\sigma_r^2 \cong \frac{1}{l}\sum_{k=1}^{l} r^2(k) \tag{11}$$

3. The variation of the innovation second-order moment:

$$\text{Slew rate} = \sigma_r^2(k) - \sigma_r^2(k-k_1) \tag{12}$$

where the parameter k_1 is positive and can be chosen by designers. Throughout the paper, we set $k_1 = 50$ and $l = 500$.

The membership functions for input variables are defined by triangular functions, due to the fact that they are suitable for statistical data and are easy to implement. The membership functions can be designed via genetic algorithms, and they are illustrated in Figs. 1, 2 and 3, respectively [2]. The output of the fuzzy tuner is the weighting factor α, as shown in Fig. 4. The basic tuning idea is given as follows. When the mean of the innovations is near zero, α

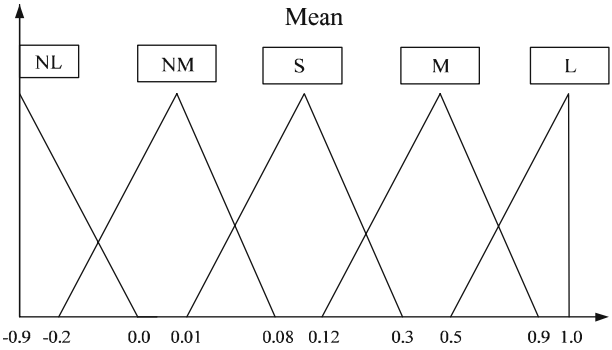

Fig. 1 Membership function for the mean of the innovations

is selected according to the moment σ_r^2 and its slew rate to tune noise the moment σ_r^2 identical to the actual noise magnitude. When the mean value moves away from zero and the second-order moment becomes large, the EIF will be unstable and a large value of α is then applied to reduce the noise moment σ_r^2 and to avoid the instability. Note that has a more direct effect on the moment σ_r^2 of the innovations, and small R results in more confident on the measurement data. This ensures that the filter can avoid divergence due to modeling errors or system uncertainties. When the mean and the moment σ_r^2 are extremely large, the readings may have some problems such that the filter cannot trust the measurements any more, and a small value of α is used. By selecting an appropriate value of α, the fuzzy tuner tunes the EIF so as to keep the innovation sequence act as a zero-mean white noise process with a suitable moment σ_r^2.

Based on the above-mentioned tuning ideas, the proposed fuzzy tuner uses 45 rules; for example, three rules are illustrated in the following;

- IF the mean is small r, AND the moment σ_r^2 is large, AND the slew rate is positive, THEN α is Medium.
- IF the mean r is large, AND the moment σ_r^2 is medium, AND the slew rate is zero, THEN α is Large.
- IF the mean r is medium, AND the moment σ_r^2 is medium, AND the slew rate is negative, THEN α is Large.

Tables 1, 2 and 3 summarizes these 45 fuzzy rules, in which negative large (NL), negative medium (NM), small (S), medium (M), large (L), positive, zero and negative represent the corresponding fuzzy sets. The proposed fuzzy tuner adopts the Mamdani-style

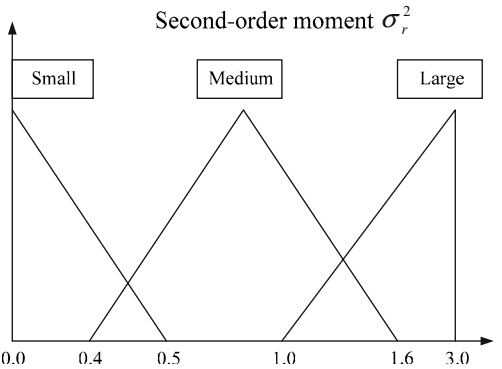

Fig. 2 Membership function for the second-order moment of the innovations

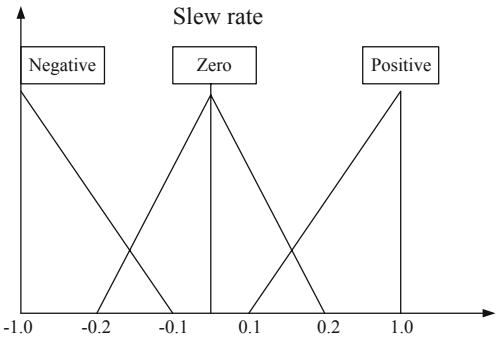

Fig. 3 Membership function for the slew rate of the second-order moment σ_r^2

inference engine and the max-min method for defuzzification. Figure 5 depicts a flow chart of the FEIF algorithm.

3 Laser Triangulation and Static Posture Estimation

3.1 Laser Triangulation

This section aims to describe a laser triangulation method using an experimental 360° laser scanner, and then propose a static posture estimation algorithm. In doing so, there must have at least three reflectors in order to uniquely determine the absolute position and orientation of the robot with respect to the reference world frame. From Fig. 6, the position and orientation of the robot, denoted by (x_c,y_c) and θ, respectively, can be derived by the triangulation method. Suppose that the positions of the three reflectors are known and located at (x_1,y_1), (x_2,y_2) and (x_3,y_3), respectively. The laser scanner detects the three bearing measurements, θ_1, θ_2 and θ_3, representing the angles from the orientation of the robot to the reflectors. The triangulation method is stated as below. Given three distinct bearing measurements, consider the following three measurement equations

$$\tan(\theta + \theta_1) = \frac{y_1 - y_c}{x_1 - x_c} \tag{13}$$

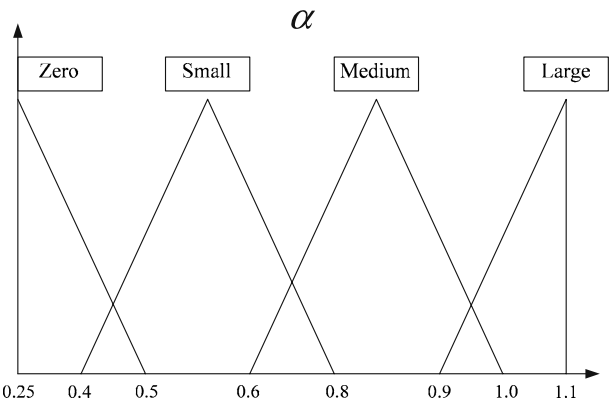

Fig. 4 Membership function for the weighting factor α

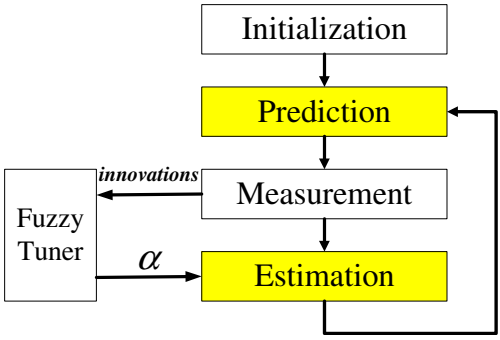

Fig. 5 Flow chart of the FEIF algorithm

$$\tan(\theta+\theta_2)=\frac{y_2-y_c}{x_2-x_c} \tag{14}$$

$$\tan(\theta+\theta_3)=\frac{y_3-y_c}{x_3-x_c} \tag{15}$$

Solving for x_c and y_c yields

$$x_c=\left[1/(m_2-m_1)\left(1+m^2\right)\right] \{(m_2m-1)[(m_1+m)x_1+(m_1m-1)y_1]\ -(m_1m-1)[(m_2+m)x_2+(m_2m-1)y_2]\} \tag{16}$$

$$y_c=\left[1/(m_2-m_1)\left(1+m^2\right)\right] \times\{(m_1+m)[(m_2+m)x_2+(m_2m-1)y_2]\ -(m_2+m)[(m_1+m)x_1+(m_1m-1)y_1]\} \tag{17}$$

where $m_1=\tan\theta_1$, $m_2=\tan\theta_2$, $m_3=\tan\theta_3$ and $m=\tan\theta$ is calculated by

$$m=\frac{(m_3-m_1)(y_1-y_2-m_1x_1+m_2x_2)-(m_2-m_1)(y_1-y_3-m_1x_1+m_3x_3)}{(m_3-m_1)(m_1y_1+x_1-m_2y_2-x_2)-(m_2-m_1)(m_1y_1+x_1-m_3y_3-x_3)} \tag{18}$$

Consequently, from Eq. 13, the orientation θ can be uniquely determined by

$$\theta=A\tan 2(y_1-y_c,x_1-x_c)-\theta_1 \tag{19}$$

Table 1 Fuzzy rule matrix for positive slew slope

σ_γ	$\overline{\gamma}$				
	NL	NM	S	M	L
S	Large	Small	Small	Small	Large
M	Large	Large	Small	Large	Large
L	Large	Large	Medium	Large	Large

Table 2 Fuzzy rule matrix for zero slew slope

σ_γ	$\overline{\gamma}$				
	NL	NM	S	M	L
S	Large	Small	Zero	Small	Large
M	Large	Medium	Small	Medium	Large
L	Large	Medium	Small	Medium	Large

where $A\tan 2(y_1-y_c, x_1-x_c)$ is the two-argument arc tangent function defined as follows;

$$A\tan 2(y_1-y_c, x_1-x_c) = \begin{cases} 0, & x_1-x_c>0,\ y_1-y_c=0 \\ \pi/2, & x_1-x_c=0,\ y_1-y_c>0 \\ 3\pi/2, & x_1-x_c=0,\ y_1-y_c<0 \\ \pi, & x_1-x_c<0,\ y_1-y_c=0 \\ \tan^{-1}\frac{y_1-y_c}{x_1-x_c}, & x_1-x_c>0,\ y_1-y_c>0 \\ \tan^{-1}\frac{y_1-y_c}{x_1-x_c}+\pi, & x_1-x_c<0,\ y_1-y_c>0 \\ \tan^{-1}\frac{y_1-y_c}{x_1-x_c}+\pi, & x_1-x_c<0,\ y_1-y_c<0 \\ \tan^{-1}\frac{y_1-y_c}{x_1-x_c}+2\pi, & x_1-x_c>0,\ y_1-y_c<0 \end{cases} \tag{20}$$

and $\tan^{-1}(\cdot)\in(-\pi/2,+\pi/2)$.

In addition, if the special conditions $\theta=\pi/2$ or $3\pi/2$, $i=1,2,3$ occur, then m_i is hardly calculated. Thus, other auxiliary equations can be utilized to solve this problem. Rearranging Eqs. (13–15) gives

$$\tan\theta_i = \frac{(y_c-y_i)-(x_c-x_i)\tan\theta}{(x_c-x_i)+(y_c-y_i)\tan\theta}, \quad i=1,2,3 \tag{21}$$

Since $\theta_i=\pi/2,3\pi2$, from Eq. 21, one can yield

$$(x_c-x_i)+(y_c-y_i)\tan\theta=0, \quad i=1,2,3 \tag{22}$$

Let $m=\tan\theta$, and rearranging Eq. 22 gives

$$y_c m - y_i m + x_c = x_i, \quad i=1,2,3 \tag{23}$$

Now, we have three cases to solve m, x_c, y_c and θ:

Case 1: if the conditions $\theta_i=\pi/2$ or $3\pi/2$, $i=1,2,3$ occurs, three equations of Eq. 23 can be applied to solve m, x_c, y_c and θ.
Case 2: if the conditions $\theta_i=\pi/2$ or $3\pi/2$, $i=1,2$ occurs, two equations of Eq. 23 and Eq. (15) can be applied to solve m, x_c, y_c and θ.

Table 3 Fuzzy rule matrix for negative slew slope

σ_γ	$\overline{\gamma}$				
	NL	NM	S	M	L
S	Medium	Small	Small	Small	Medium
M	Large	Large	Small	Large	Large
L	Large	Large	Medium	Large	Large

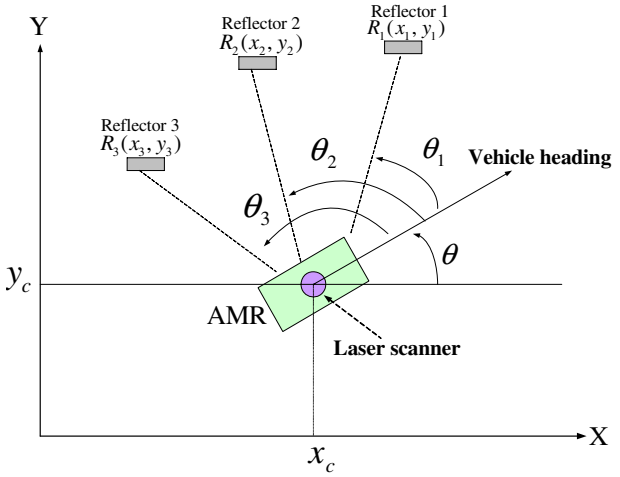

Fig. 6 Illustration of laser triangulation using the laser scanner and three reflectors

Case 3: if the conditions $\theta_i = \pi/2$ or $3\pi/2$ holds, one equation of Eq. 23 and Eqs. 14–15 can be applied to solve m, x_c, y_c and θ.

Before closing this section, the proposed three-point triangulation method is summarized as follows; given three distinct and exact bearing measurements θ_1, θ_2 and θ_3, the position and orientation of the robot can be uniquely determined without errors.

3.2 Static Posture Estimation

This section presents a static posture estimation algorithm for the AMR based on the laser scanning measurements. Figure 7 shows the locations of the AMR and three more reflectors, where p denotes the number of the reflectors installed on the surrounding walls of the workspace. In this scenario, the laser scanner mounted on the AMR takes a 360° scanning to measure all the bearings of the reflectors with respect to the orientation of the AMR. Note that all the bearings' measurement errors are realistically assumed to be white Gaussian processes with zero mean. To obtain a better pose estimate of the AMR with respect to the reference frame, the algorithm is divided into two stages: the first stage is an

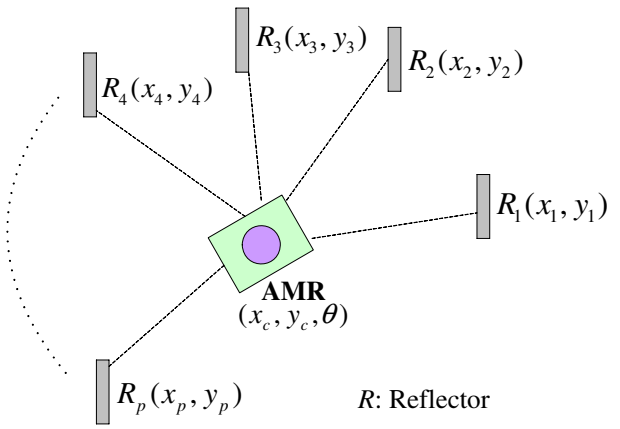

Fig. 7 Illustration of the locations of the robot and p reflectors

initial estimation utilizing the three-point triangulation presented in the previous section, and the second stage is a precise estimation utilizing FEIF to fuse all the reflectors' readings.

Stage 1: Initial Posture Estimation (Three-point Triangulation)

Step 1: Select three distinct reflectors whose mutually separate angles are as large as possible, and perform the measurements of their bearings with respect to the orientation of the AMR n times to obtain n sets of three measured values, $\theta_1(i)$, $\theta_2(i)$ and $\theta_3(i)$, $i=1, 2, 3,.., n$.

Step 2: Apply a simple averaging method to obtain the means of θ_1, θ_2 and θ_3 as follows;

$$\overline{\theta}_1 = \frac{1}{n}\sum_{i=1}^{n}\theta_1(i), \quad \overline{\theta}_2 = \frac{1}{n}\sum_{i=1}^{n}\theta_2(i), \quad \overline{\theta}_3 = \frac{1}{n}\sum_{i=1}^{n}\theta_3(i)$$

Step 3: Calculate the corresponding terms: $m_1 = \tan\overline{\theta}_1, m_2 = \tan\overline{\theta}_2$ and $m_3 = \tan\overline{\theta}_3$, respectively, and obtain the initial estimate of the robot pose $\left(\widehat{x}_c, \widehat{y}_c, \widehat{\theta}\right)$ using Eqs. 16–19.

Stage 2: Precise Posture Estimation (FEIF-based Sensor Fusion)

In applying the FEIF to significantly reduce the initial estimation error in the first stage, a state equation describing the static pose of the AMR is required and simply expressed by

$$X(k+1) = X(k)$$

or,

$$\begin{bmatrix} x_c(k+1) \\ y_c(k+1) \\ \theta(k+1) \end{bmatrix} = \begin{bmatrix} x_c(k) \\ y_c(k) \\ \theta(k) \end{bmatrix} \tag{24}$$

The bearing measurements from the all reflectors are rewritten is a vector form.

$$Z(k) = h(X(k)) + V(k) \tag{25}$$

or,

$$\begin{bmatrix} \theta_1(k) \\ \theta_2(k) \\ \vdots \\ \theta_p(k) \end{bmatrix} = \begin{bmatrix} A\tan 2[y_1 - y_c(k), x_1 - x_c(k)] - \theta(k) \\ A\tan 2[y_2 - y_c(k), x_2 - x_c(k)] - \theta(k) \\ \vdots \\ A\tan 2\left[y_p - y_c(k), x_p - x_c(k)\right] - \theta(k) \end{bmatrix} + \begin{bmatrix} v_1(k) \\ v_2(k) \\ \vdots \\ v_p(k) \end{bmatrix} \tag{26}$$

where the function $A\tan 2(\cdot,\cdot)$ is defined in Eq. 20, the measurement noises $v_1(k)$, $v_2(k)$, , $v_p(k)$ are assumed to be mutually independent, zero-mean white Gaussian processes with a covariance matrix $R(k) = \mathrm{diag}\{\sigma_{v1}^2, \sigma_{v2}^2, \cdots, \sigma_{vp}^2\}$. In order to obtain the best pose estimate of the mobile robot, a discrete-time FEIF-based posture estimation algorithm is proposed in the following.

Step 1: Initialization. Select $\beta=-2$, initial values of the information state $\widehat{y}_\alpha(0|0)$ and the information matrix $Y_\alpha(0|0)$ at time $k=0$. Note that $\widehat{y}_\alpha(0|0) = Y_\alpha(0|0)\widehat{X}(0|0)$ where $\widehat{X}(0|0) = [\widehat{x}(0|0), \widehat{y}(0|0), \widehat{\theta}(0|0)]^T$.

Step 2: One-step Prediction. Let the optimal information estimate at time k be $\widehat{y}_\alpha(k/k)$ and its information matrix be $Y_\alpha(k/k)$. Use Eqs. 27–28 to calculate the best prediction, $\widehat{y}_\alpha(k+1|k)$ and its information state vector $Y_\alpha(k+1|k)$.

$$\widehat{y}_\alpha(k+1|k) = Y_\alpha(k+1|k)Y_\alpha^{-1}(k|k)\widehat{y}_\alpha(k|k) \tag{27}$$

$$Y_\alpha(k+1|k) = Y_\alpha(k|k) \tag{28}$$

Step 3: Generation of the weighting factor α from the fuzzy tuner. The localization controller reads a new data $Z(k+1)$, calculates the innovation $r(k+1)$ using Eq. 29 and uses the fuzzy tuning algorithm to generate an appropriate α.

Step 4: Estimation (Measurement Update).

At time $k+1$, the localization controller reads the incoming measurement data $Z(k+1)$ and then uses Eqs. 7–8 to obtain the updating information state estimate $\widehat{y}_\alpha(k+1|k+1)$ and information matrix $Y_\alpha(k+1|k+1)$. The innovation $r(k+1)$ is given by

$$r(k+1) = Z(k+1) - h\left(\widehat{X}(k+1|k)\right) \tag{29}$$

Furthermore, the Jacobian matrix of $\nabla\overline{h}_X(k+1)$ evaluated at $\widehat{X}(k+1|k) = Y_\alpha(k+1|k)^{-1} \times \widehat{y}_\alpha(k+1|k)$ is given by

$$\nabla h_X(k+1) = \frac{\partial h}{\partial X}\bigg|_{X=\widehat{X}(k+1|k)} = \begin{bmatrix} \frac{y_1-y_c}{(x_1-x_c)^2+(y_1-y_c)^2} & \frac{x_c-x_1}{(x_1-x_c)^2+(y_1-y_c)^2} & -1 \\ \frac{y_2-y_c}{(x_2-x_c)^2+(y_2-y_c)^2} & \frac{x_c-x_2}{(x_2-x_c)^2+(y_2-y_c)^2} & -1 \\ \vdots & \vdots & \vdots \\ \frac{y_p-y_c}{(x_p-x_c)^2+(y_p-y_c)^2} & \frac{x_c-x_p}{(x_p-x_c)^2+(y_p-y_c)^2} & -1 \end{bmatrix} \tag{30}$$

Step 5: Repeat Step 2 to Step 4.

4 Pose Tracking

In fact, the proposed triangulation method in the previous section can not be directly applied to obtain the correct pose of a moving AMR at any speed unless the laser scanner takes an infinite rotation speed. In realistic situations, the laser scanner has the scanning speed at the rate of 6.0 rev/sec such that the proposed triangulation method fails to keep trace of continuous poses of the AMR. This is because the poses of the moving AMR are distinct at the time instants while the laser scanner is detecting any retro-reflectors. Worthy of mention is that the proposed triangulation method is very useful for the pose initialization problem which is encountered not only at start-up, but also during operation for robot pose recovery in case of pose tracking failures.

To circumvent the aforementioned difficulty, only one laser bearing measurement, not three measurements, along with the odometric information from the two driving wheels is employed to update the continuous poses of the AMR via the proposed FEIF-based pose tracking method. Figure 8 shows the angular measurements of the four reflectors one by one. Notice that the odometric information is easily obtained from two encoders amounted on the driving motors. The proposed pose tracking method will work well once the proposed triangulation method has been adopted to find an almost correct initial robot pose.

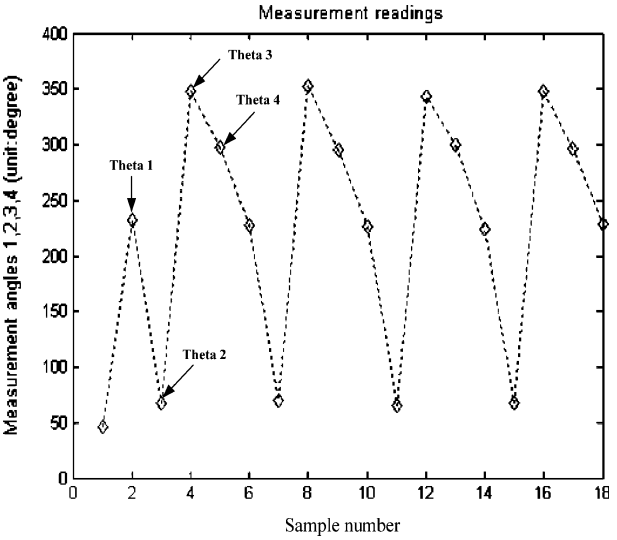

Fig. 8 Angular measurements of the four reflectors

The proposed pose tracking algorithm will also perform well for an autonomous robot with differential driving at speeds less than 1.0 m/s. This is due to the validity of the robot's kinematic model, which has been shown valid for speeds less than 1.0 m/s. If a dynamic model of the robot is used, then the proposed pose tracking algorithm can be applicable to find the continuous robot's pose at any admissible speeds.

With proven estimation accuracy and robustness, the fuzzy extended information filtering (FEIF) method is again used in the section to estimate the continuous pose of the AMR by employing only one bearing measurement to accomplish the posture tracking goal. Hence, the measurement equation now becomes

$$z(k) = h_1(X(k)) + v(k) \tag{31}$$

where

$$X(k) = \begin{bmatrix} x_c(k) \\ y_c(k) \\ \theta(k) \end{bmatrix},\ z(k) = [\theta(k)],$$

$$h_1(X(k)) = [A\tan 2[y_i - y_c(k), x_i - x_c(k)] - \theta(k)],\ i = 1, 2, \cdots, p.$$

Furthermore, the measurement noise, *v(k)*, is again assumed to be an independent, zero-mean white Gaussian process with variance σ_v^2.In fact, one reflector reading is insufficient and will result in slow convergent rate, but if the number of the reflectors is large, then a better estimate can be obtained. To fuse the laser scanner's reading with the odometer information from the driving wheels, the kinematics model of the robot with two differential driving wheels and pure rolling is needed and described by the following nonlinear state equation

$$\frac{d}{dt}\begin{bmatrix} x(t) \\ y(t) \\ \theta(t) \end{bmatrix} = \begin{bmatrix} v_c(t)\cos\theta(t) \\ v_c(t)\sin\theta(t) \\ \omega_c(t) \end{bmatrix} \tag{32}$$

where $v_c(t)$ is the linear velocity and $\omega_c(t)$ is the angular velocity of the AMR. The discrete-time nonlinear state equation with an additive noise can be obtained by applying the Euler's formula to Eq. 32.

$$X(k+1) = f_1(X(k)) + W(k) \tag{33}$$

or,

$$\begin{bmatrix} x(k+1) \\ y(k+1) \\ \theta(k+1) \end{bmatrix} = \begin{bmatrix} x(k) + \Delta d \cos\theta(k) \\ y(k) + \Delta d \sin\theta(k) \\ \theta(k) + \Delta\theta \end{bmatrix} + \begin{bmatrix} w_x(k) \\ w_y(k) \\ w_\theta(k) \end{bmatrix} \tag{34}$$

where $\Delta d = \Delta T \cdot v_c$, $\Delta\theta = \Delta T \cdot \omega_c(t)$, ΔT is the time between two successive reflectors' detections; noise processes, $w_x(k)$, $w_y(k)$ and $w_\theta(k)$, denote the errors due to the wheel slippage, surface roughness, etc., and they are modeled as uncorrelated zero-mean white Gaussian processes with a covariance matrix $Q(k) = \text{diag}\left\{\sigma_{wx}^2, \sigma_{wy}^2, \sigma_{w\theta}^2\right\}$, i.e., $W(k) \sim N(0, Q(k))$. In fact, one bearing reading during one sampling interval is insufficient and thus results in estimation errors and slow convergence rates. Therefore, it is anticipated that more angle readings will result in pose estimation. In what follows proposes a real-time FEIF algorithm.

Step 1: Initialization. Select β=–2, initial values of the information state $\hat{y}_\alpha(0|0)$ and the information matrix $Y_\alpha(0|0)$ at time k=0. Note that the initial information state is given by $\hat{y}_\alpha(0|0) = Y_\alpha(0|0)\hat{X}(0|0)$ where $\hat{X}(0|0) = [\hat{x}(0|0), \hat{y}(0|0), \hat{\theta}(0|0)]^T$.

Step 2: One-step Prediction. Let the optimal estimate of $Y_\alpha(k)$ at time k be $\hat{y}_\alpha(k|k)$ and its information matrix be $Y_\alpha(k+1|k)$. Use Eqs. 5–6 to calculate the best prediction, $\hat{y}_\alpha(k+1|k)$ and its information state vector $Y_\alpha(k+1|k)$, where the Jacobian matrix $\nabla f_{1_X}(k-1)$ is given by

$$\nabla f_{1_X}(k-1) = \left.\frac{\partial f_1}{\partial X}\right|_{X=\hat{X}(k-1|k-1)} = \begin{bmatrix} 1 & 0 & -\Delta d \sin\theta \\ 0 & 1 & \Delta d \cos\theta \\ 0 & 0 & 1 \end{bmatrix} \tag{35}$$

Step 3: Generation of the weighting factor α from the fuzzy tuner. The localization controller reads a new bearing measurement $Z(k)$, computes the new innovation $r(k+1)$ and uses the fuzzy tuning algorithm to find an appropriate α.

Step 4: Estimation (Measurement Update). At time $k+1$, the localization controller reads the incoming measurement data $Z(k+1)$ and then uses Eqs. 7–8 to obtain the updating information state estimate $\hat{y}_\alpha(k+1|k+1)$ and information matrix $Y_\alpha(k+1|k+1)$, where the Jacobian matrix $\nabla h_X(k)$ is now replaced by $\nabla h_{1X}(k)$.

$$\nabla h_{1X}(k) = \left.\frac{\partial h_1}{\partial X}\right|_{X=\hat{X}(k|k-1)} = \left[\frac{y_1 - y_c}{(x_1 - x_c)^2 + (y_1 - y_c)^2} \quad \frac{x_c - x_1}{(x_1 - x_c)^2 + (y_1 - y_c)^2} \quad -1\right], \; i = 1, 2, \cdots, p. \tag{36}$$

Simultaneously, use Eq. 29 to compute the mean and covariance of the innovation $r(k)$ and detect the degree of filter divergence by the fuzzy tuner.

Step 5: Repeat Step 2 to Step 4.

Notice that if the robot failed to pose tracking, then initialization can be easily done using the proposed triangulation method presented in Section 3, assuming that the vehicle move slowly or stops at a certain position.

5 Simulations, Experimental Results and Discussion

In this section, simulation and experimental results are performed to examine the performance of the proposed laser posture estimation and tracking algorithms. Three computer simulations using MATLAB codes investigated the effectiveness of the proposed posture estimation and tracking algorithms while noise variation and modeling errors occurred. Four experiments were conducted to verify the performance of the proposed FEIF-based posture estimation and tracking algorithms of the AMR using the laser scanner and three reflectors. The last two experiments compared the performance of the EIF-based and FEIF-based posture tracking algorithms.

5.1 Computer Simulations and Discussion

Simulation 1 this simulation was used for illustration of the proposed static posture estimation method. It is assumed that the AMR equipped with a laser scanner was in a 1,000 cm × 1,000 cm square workspace, and in the surrounding space eight reflectors were installed whose positions are respectively (x_1, y_1)=(560 cm, 920 cm), (x_2, y_2)=(160 cm, 920 cm), (x_3, y_3)=(160 cm, 520 cm), (x_4, y_4)=(160 cm, 120 cm), (x_5, y_5)=(560 cm, 120 cm), (x_6, y_6)=(960 cm, 120 cm), (x_7, y_7)=(960 cm, 520 cm), (x_8, y_8)=(960 cm, 920 cm). The bearing measurements of the reflectors were corrupted with noise processes modeled as a zero-mean identical white Gaussian vector process with a covariance matrix $R(k) = \text{diag}\{\sigma_{v1}^2, \sigma_{v2}^2, \cdots, \sigma_{vp}^2\}$, where $\sigma_{v_1} = \sigma_{v_2} = \sigma_{v_3} = \sigma_{v_4} = \sigma_{v_5} = \sigma_{v_6} = \sigma_{v_7} = \sigma_{v_8} = 0.020$ rad (1.146°).The true position and orientation of the AMR were given by (x_c, y_c, θ)=(580 cm, 555 cm, 50°). To compare the proposed FEIF with the conventional EIF, one assumes that both filters take the same but incorrect covariance matrix, i.e., $R(k) = \text{diag}\{\sigma_{v1}^2, \sigma_{v2}^2, \cdots, \sigma_{vp}^2\}$, and $\sigma_{v_1} = \sigma_{v_2} = \sigma_{v_3} = \sigma_{v_4} = \sigma_{v_5} = \sigma_{v_6} = \sigma_{v_7} = \sigma_{v_8} = 0.050$ rad (2.866°). With the static posture estimation algorithm, Fig. 9(a) compares the true and estimated positions of the AMR and Fig. 9(b) depicts the time history of the estimated and true orientations of the AMR. In Fig. 9(a), the circle represents the true position, the triangle means the initial estimate using the three-point triangulation, the cross represents the EIF estimate, and the star inside the circle denotes the more accurate estimate obtained from the FEIF-based sensor fusion algorithm. The results in Fig. 9 reveal that the pose estimate using the first stage algorithm had errors due to measurement noise and finite measurements, but the FEIF-based precise estimation method in the second stage significantly reduced the errors and obtained the optimal final posture estimate $(\widehat{x}_c, \widehat{y}_c, \widehat{\theta}) = (580.25 \text{ cm}, 554.75 \text{ cm}, 49.993^\circ)$ with the steady-state pose errors of (−0.25 cm, 0.25 cm, 0.007°).

Simulation 2 this simulation aimed at observing the performance of the posture tracking algorithm for the AMR where the measurement noise varies with the smoke or mist in the air, or other light interferences. The four reflectors' positions were respectively amounted at (x_1, y_1)=(270 cm, 275 cm), (x_2, y_2)=(203 cm, 273 cm), (x_3, y_3)=(150 cm, 243 cm), and (x_4, y_4)=(260 cm, 196 cm). The initial pose of the AMR was $X(0)$=[140 cm, 200 cm, 14.9°]^T, the initial information state and information matrix were respectively $\widehat{y}_\alpha(0|0) = [1.5, 1.9, 0]^T$ and $Y_\alpha(0|0) = \text{diag}\{0.01,\ 0.01,\ 0.01\}$. Moreover, $Q = \text{diag}\{0.0001,\ 0.0001,\ 0.00001\}$, and $R = \sigma_v^2 = 0.0002$. Since the robot was moving along its predetermined path, all the bearings from the reflectors could not be taken at the same time. Hence, only one reflector bearing reading was assumed to obtain at a sampling instant. The AMR was assumed to move along a line path with a constant velocity v_c= 1 cm/s so that Δd= 1*ΔT cm and $\Delta\theta$= 0° in Eq. 34, where ΔT is the time between two successive reflectors' detections. The measurement

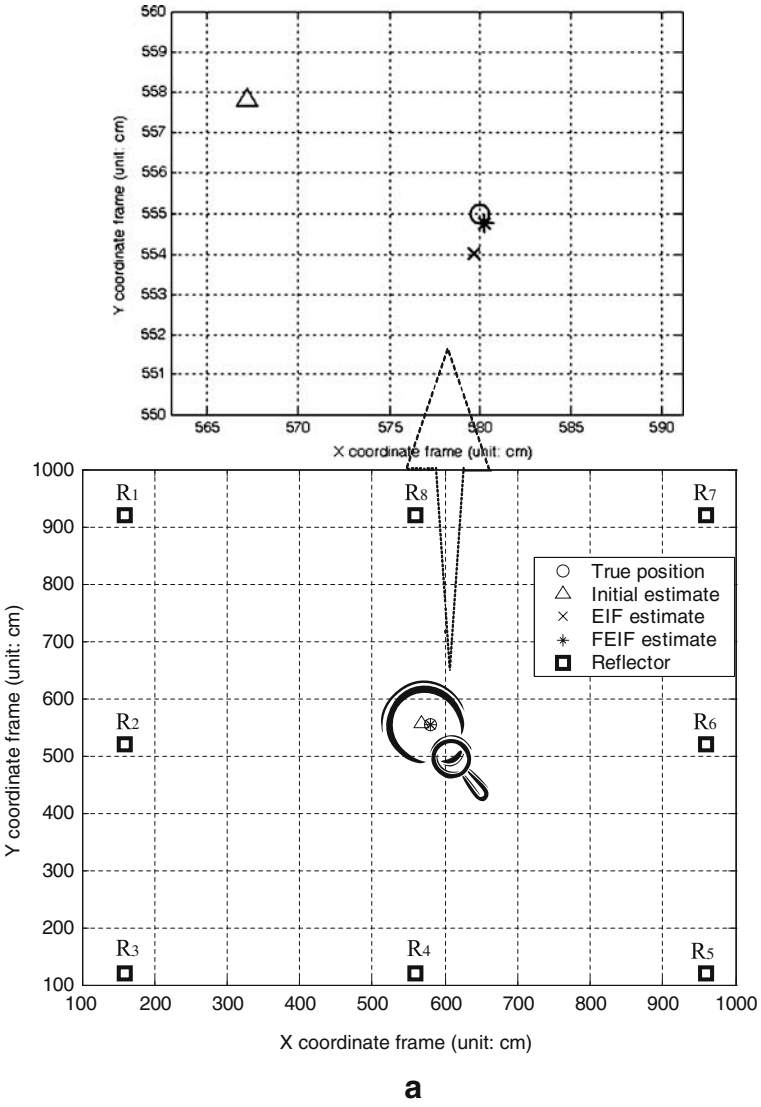

Fig. 9 **a** Comparisons of the true and estimated positions of the AMR. **b** Comparisons of the true and estimated orientations of the AMR

noise covariance was actually changed up to $R = 0.02$ after the 2,400th sample. The innovations of the reflector measurements are depicted in Fig. 10, where the innovations became large after the 2,400th sample due to the noise variation. The true and estimated states of the AMR are shown in Fig. 11. Since the noise parameters, Q and R, in FEIF are able to adapt to the actual noise characteristics, we observe in Fig. 11 that the FEIF has a better estimation performance than the EIF while noise variation occurs.

Simulation 3 this simulation focused on exploring the performance of the posture tracking of the robot while the modeling errors occur. Four reflectors were respectively installed at $(x_1 y_1)$=(75 cm, 50 cm), $(x_2 y_2)$=(200 cm, 340 cm), $(x_3 y_3)$=(450 cm, 120 cm) and $(x_4 y_4)$=

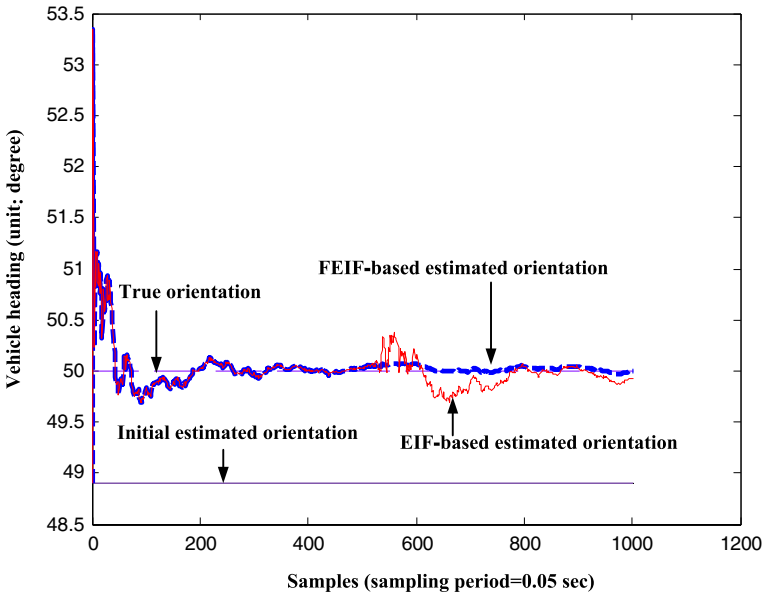

Fig. 9 (Continued)

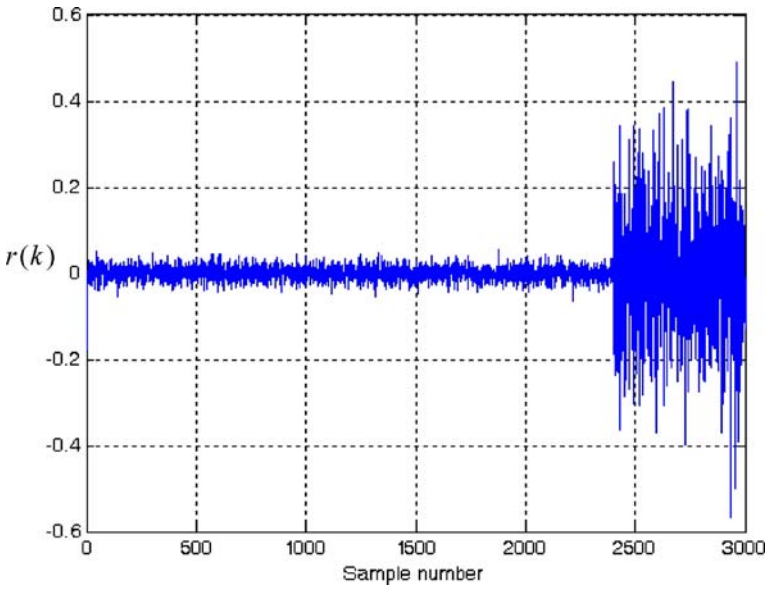

Fig. 10 The behavior of the innovations, $r(k)$, of the reflector measurements

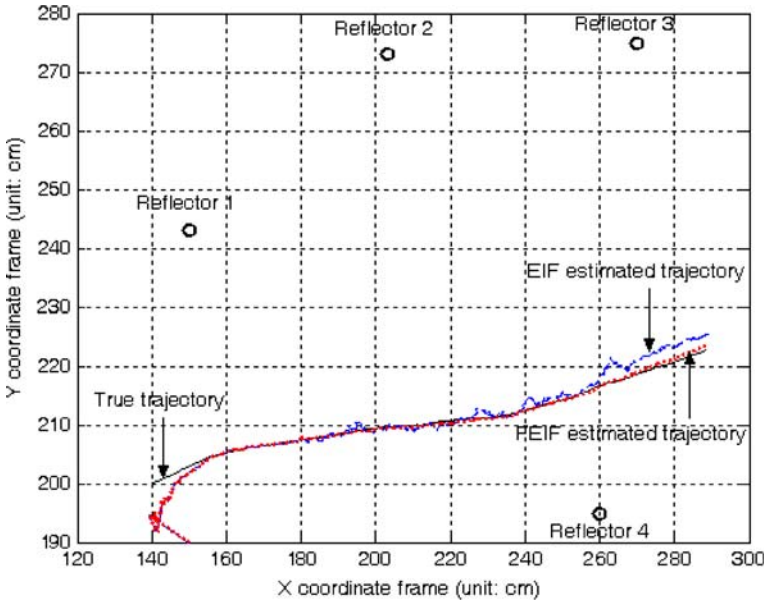

Fig. 11 Simulated results of the true and estimated positions of the AMR while noise variations occur

(350 cm, 0 cm). The initial pose of the robot was set by $\widehat{X}(0) = [150\text{ cm } 150\text{ cm } 5.73^\circ]^T$, and the initial information state and information matrix were given by $\widehat{y}_\alpha(0|0) = [1.25, 1.75, 0]^T$ and $Y_\alpha(0|0) = diag\,\{0.01, 0.01, 0.01\}$. The values of noise covariance matrices were set by R=0.0001 and Q=diag{0.0001, 0.0001, 0.00001}. The sampling interval is ΔT=0.05 s, and the AMR traveled along a line path with constant unit velocity so that Δd=0.05 cm and $\Delta\theta$=0 in Eq. 34. The robot was expected to navigate along a certain direction with constant velocity, but it had an abrupt acceleration and made a sharp turn (Δd=0.2, $\Delta\theta$=0.005) actually after the 1,500th sample. Hence, the modeling error occurred due to the difference between the filter's internal model and the actual model. It is observed that the means of the innovations in the EIF move away from zero, but the means in the FEIF still remain zero after a short computation time, while modeling errors occur. Figure 12 displays the true and estimated states of the robot. The results in Fig. 12 indicate that the FEIF has a better robustness property than the EIF under the occurrence of modeling errors.

5.2 Experimental Results and Discussion

Experiment 1 the first experiment was performed to investigate the validity and accuracy of the proposed triangulation localization method for the AMR. The real range and bearing measurements are corrupted with measurement noise. For the static posture determination of the AMR, Fig. 13 depicts the schematic diagram of the experiment laser scanner and reflectors. The four reflectors were installed at the positions pre-specified by $(x_1 y_1)$= (320 cm, 310 cm),$(x_2 y_2)$=(190 cm, 310 cm), $(x_3 y_3)$=(190 cm, 180 cm) and $(x_4 y_4)$= (320 cm, 180 cm) with respect to the reference world frame. The robot was precisely located at different eight positions inside the square space surrounded by the reflectors in order to examine the accuracy of the proposed method. These eight true positions and

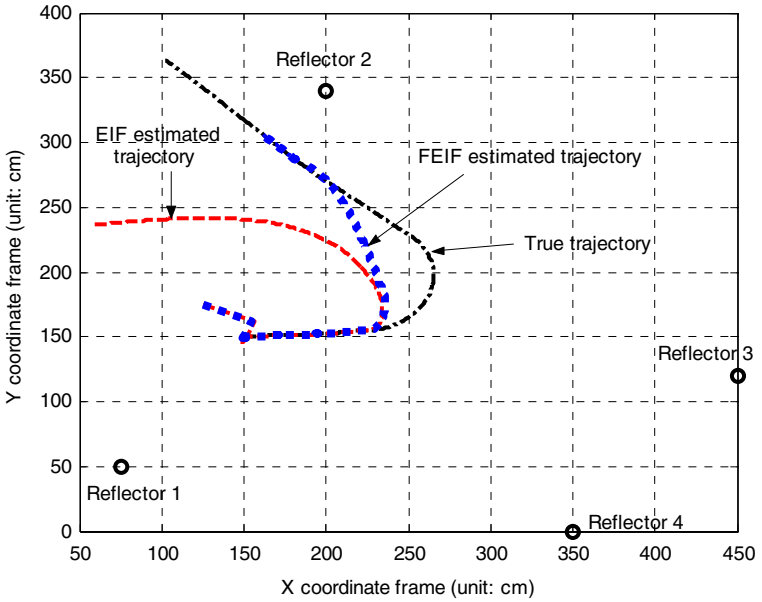

Fig. 12 Simulated results of the true and estimated positions of the AMR while modeling errors occurs

orientations of the robot were depicted in Table 4 and their heading angles were given by 0°, 45°, 90°, 135°, 180°, 225°, 270° and 315°, respectively.

While the experiment was being performed, the statistical properties of bearing measurements from the all reflectors were well evaluated in order to investigate the nature of the measurement noise processes in Eq. 25. The real noise processes $v_1(k)$, $v_2(k)$, $v_3(k)$ and $v_4(k)$ are indeed shown to be mutually independent and Gaussian ones with a zero vector-valued mean and a covariance matrix $R(k) = \text{diag}\{\sigma_{v1}^2, \sigma_{v2}^2, \sigma_{v3}^2, \sigma_{v4}^2\}$, where σ_{vi}=0.0262 rad for i=1,.., 4. Table 4 shows the experimental results for the static robot posture estimation of

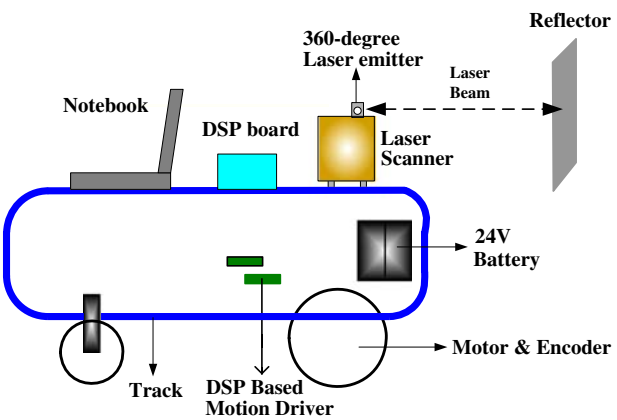

Fig. 13 Schematic diagram of experimental mobile robot and laser scanner

Table 4 Experimental results of the static robot posture estimation at eight positions and orientations

Parameter	Value			
The first four poses				
True positions (x_c,x_c) cm	(253,245)	(280,234)	(266,267)	(277,279)
True orientations θ (degree)	θ°	45°	90°	135°
Estimated positions ($\widehat{x}_c$,$\widehat{y}_c$) cm	(254.36,244.89)	(280.86,234.35)	(266.25,267.26)	(277.54,279.42)
Estimated orientations $\widehat{\theta}$ (degree)	1.88°	44.13°	91.19°	135.62°
x-axis errors $\lvert\widehat{x}_c - x_c\rvert$	1.36 cm	0.86 cm	0.25 cm	0.42 cm
y-axis errors $\lvert\widehat{y}_c - y_c\rvert$	0.11 cm	0.35 cm	0.26 cm	0.42 cm
Orientation errors $\lvert\widehat{\theta} - \theta\rvert$	1.88°	0.87°	1.19°	0.62°
The last four poses				
True positions (x_c, y_c) cm	(225,221)	(221,264)	(260,213)	(230,241)
True orientations θ (degree)	180°	225°	270°	315°
Estimated positions ($\widehat{x}_c$,$\widehat{y}_c$) cm	(225.31,222.49)	(221.03,263.94)	(260.76,212.38)	(231.18,241.77)
Estimated orientations $\widehat{\theta}$ (degree)	181.34°	226.29°	271.67°	315.82°
x-axis errors $\lvert\widehat{x}_c - x_c\rvert$	0.31 cm	0.03 cm	0.76 cm	1.18 cm
y-axis errors $\lvert\widehat{y}_c - y_c\rvert$	1.49 cm	0.06 cm	0.62 cm	0.77 cm
Orientation errors $\lvert\widehat{\theta} - \theta\rvert$	1.34°	1.29°	1.67°	0.82°

the robot located at eight positions and orientations. The results in Table 4 indicate that the proposed triangulation method is proven capable of having a maximal position error of less than 1.5 cm and a maximal orientation error of less than 2°.

Experiment 2 the second experiment was conducted to explore the feasibility and performance of the proposed static posture estimation algorithm. Moreover, the experiment aimed at studying what accuracy the proposed algorithm achieves. Figure 14(a) shows the block diagram of the experimental 360-degree laser scanner, and Fig. 14(b) displays the picture of the experimental laser scanner. For the experimental setup, the laser scanner mounted on the robot was located at the position (−134 cm, 35 cm, 90°) and the three laser reflectors were prespecified at three three-dimensional positions: P1 (0 cm, 0 cm, 59 cm), P2 (−20 cm, 110 cm, 59 cm), P3 (−200 cm, 0 cm, 59 cm) with respect to the world frame. While the experiments were being performed, two encoders' outputs were used to fuse with the angle readings from the laser scanner. Before proceeding with the experiments, all important components, such as the laser scanner and the dead-reckoning module were correctly calibrated. The FEIF-based posture estimation algorithm using standard C++ programming techniques was implemented on an Intel Pentium 586 PC. The proposed laser scanner is efficiently designed to detect the existence of any reflector around the robot's environment within approximately 60 μs, depending upon the response tine of the photo detector. The detected signal is quickly interfaced to the host PC via digital input/output device and then processed by the PC. In comparison with the speed of the autonomous mobile robot (less than 1 m/s) and the rotation speed of the scanner (6 rev/s), this communication delay between the proposed laser scanner and the host PC is rather small and can be ignored. However, if the robot navigates around its working environment at vary fasts speeds (>>100 cm/s), the communication delay would be taken into account. The initial settings of $Y_\alpha(0/0) = \mathrm{diag}\{1/20,\ 1/20,\ 1/5\}$, $R = 0.001$ and $Q = \mathrm{diag}\{0.01,\ 0.01,\ 0.001\}$ were considered for initializing the FEIF. Figure 15 depicts the behavior of the proposed static robot pose estimates, assuming the initial pose estimate be

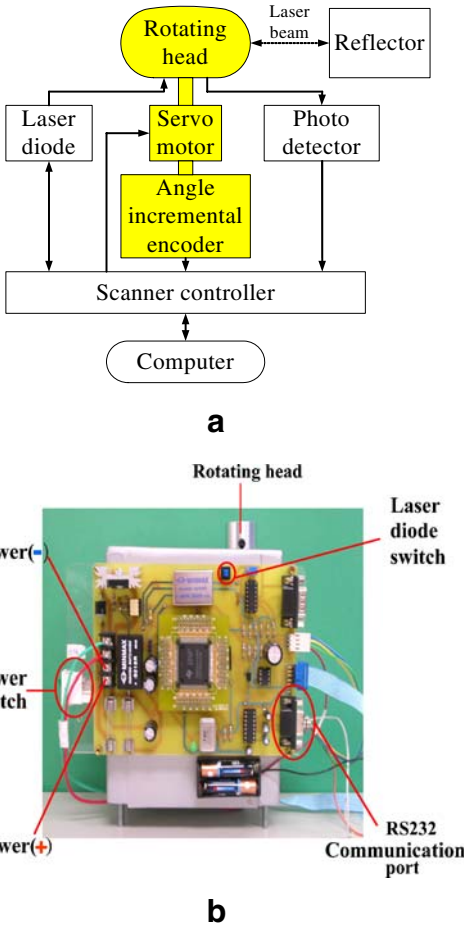

Fig. 14 **a** Block diagram of the experimental laser scanner. **b** The picture of the experimental laser scanner

$\widehat{X}(0/0) = [-100\text{ cm}, 80\text{ cm}, 102^\circ]^T$. As can be seen in Fig. 15, the pose estimates of the robot quickly converged to their actual position. In this experiment, if the initial condition of $\widehat{X}(0/0)$ is far from its true position, and then the FEIF may not succeed to converge to the actual values. Note that if the initial state condition of $\widehat{X}(0/0)$ is unknown, it can be easily obtained using the first stage algorithm based on the triangulation method presented in Section 3. To find the accuracy and precision of the estimates, the actual values of the robot's pose were precisely measured by hand and the steady-state pose tracking errors were (−0.086 cm, −0.067 cm, 0.25°). The experimental result indicates that the proposed posture estimation method can be effectively and precisely used to find the static pose of the robot.

Experiment 3 the third experiment was used for evaluating the performance of the EIF-based posture tracking algorithm when the robot navigated along a line path in a structured environment with a flat, partly smooth surface and a magnetic interference source. All initial parameter settings and the initial state were identical to the previous set-up, but the robot moved at a constant linear velocity $v_c = 1$ cm/s with the vehicle heading of 86.45°. Figure 16 displays the time history of the continuous EIF-based robot's posture estimates,

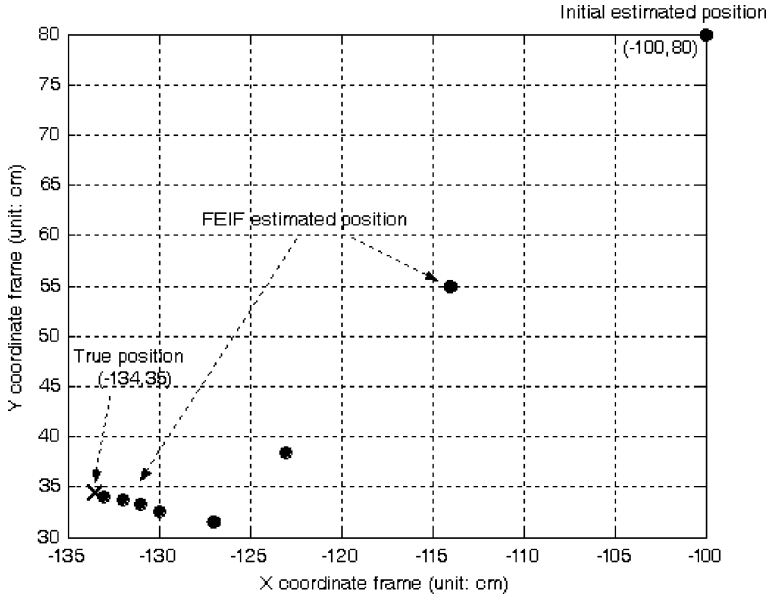

Fig. 15 Static robot position estimates using the laser posture estimation algorithm

assuming the initial estimate be $\widehat{X}(0/0) = [-87\text{cm}, 135\text{cm}, 99°]^T$. Observe in Fig. 16 that the steady-state pose tracking error was (−0.14 cm, −0.14 cm, 1.15°) for the robot with straight-line movement parallel to the y-axis.

Experiment 4 the fourth experiment was used for evaluating the moving performance of the proposed FEIF-based posture tracking algorithm when the robot moved along the same path as in Experiment 3. All initial parameter settings and the initial state were identical to the previous experiment. The constant linear velocity of the robot was v_c= 1 cm/s and the vehicle heading was 90°. Figure 17 depicts the time history of the FEIF-based robot's posture estimates. To find the accuracy and precision of the estimates, the actual values of the robot's pose were precisely measured by hand and the steady-state pose tracking errors were (−0.018 cm, 0.012 cm, 0.0135).

Through the last two experimental results, we observe that the FEIF-based estimates have precisely converged to the actual robot posture estimates when the robot moved along a line path. Actually, we have also shown that the FEIF outperforms the EIF in the case of robot position and orientation recovery at slow speeds.

Experiment 5 The four reflectors' positions were respectively amounted at (x_1,y_1)=(162 cm, 325 cm), (x_2,y_2)=(305 cm, 345 cm), (x_3,y_3)=(310 cm, 242 cm) and (x_4,y_4)=(190 cm, 212 cm). In the experiment, the initial pose of the AMR was set by $\widehat{X}(0) = [255\text{ cm}, 210\text{ cm}, 28.6°]^T$, and the AMR was steered to move along a circle path with a constant velocity v_c= 1 cm/s. Figure 18 depicts the time history of the FEIF-based robot's posture estimates. The result in Fig. 18 shows that the proposed posture tracking algorithm is shown to have satisfactory estimation performance and is able to adapt to the actual noise characteristics.

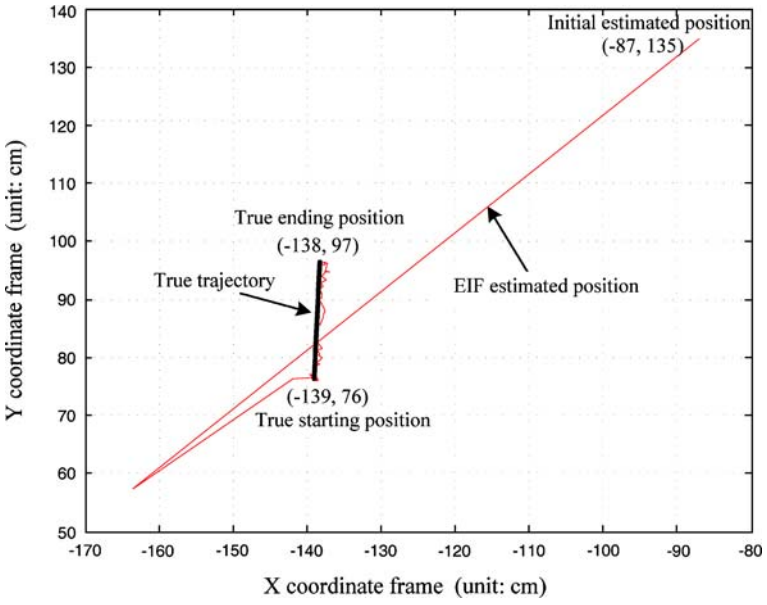

(a)

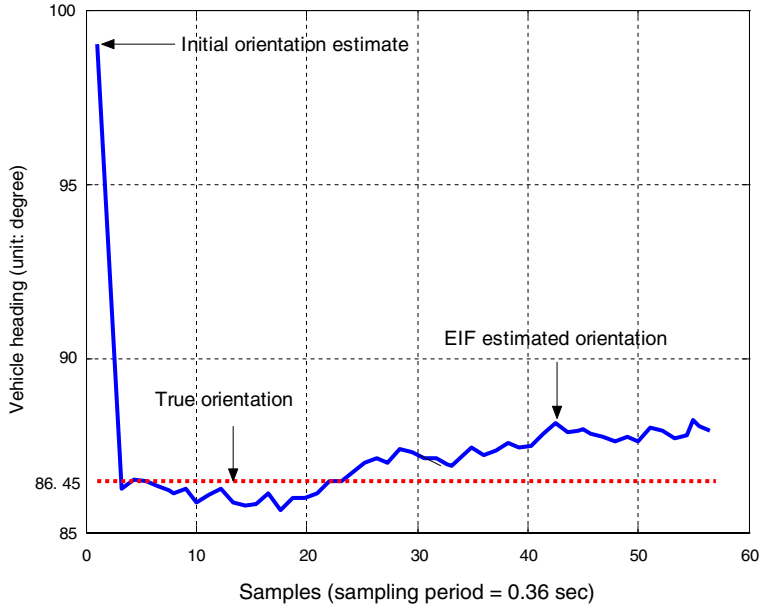

(b)

Fig. 16 The laser EIF-based posture tracking algorithm. **a** Robot position estimates. **b** Behavior of the vehicle heading estimate of the navigating robot

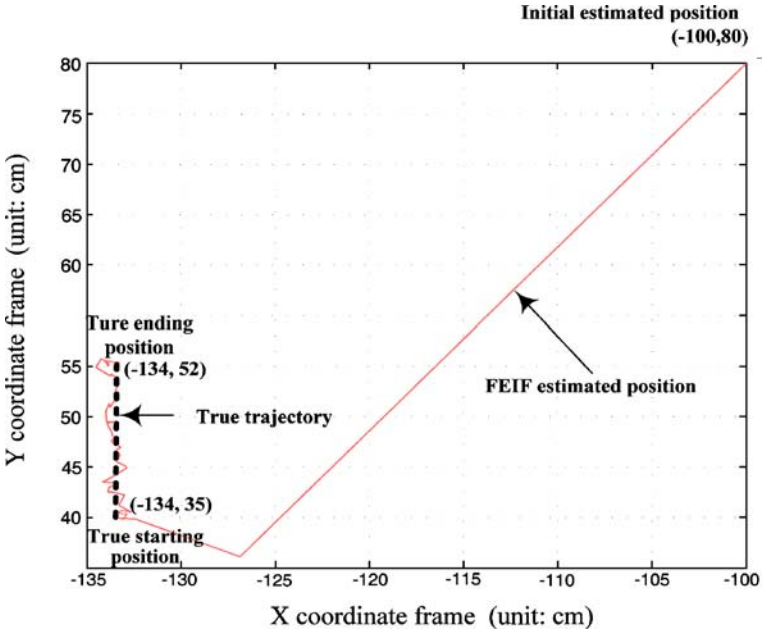

(a)

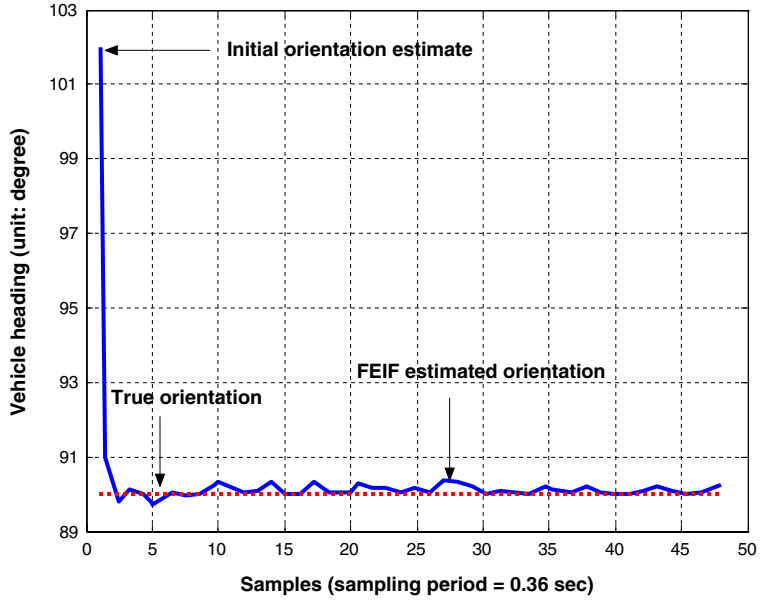

(b)

Fig. 17 The laser FEIF-based posture tracking algorithm. **a** Robot position estimates. **b** Behavior of the vehicle heading estimate of the navigating robot

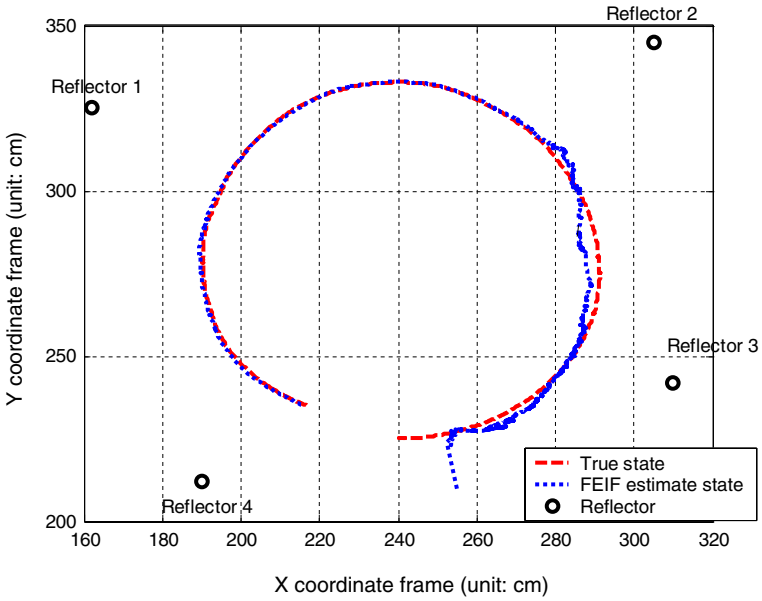

Fig. 18 Robot position estimates of the proposed pose tracking algorithm while the AMR was steered to move along a circle path

6 Conclusions

This paper has presented posture estimation and tracking methods using fuzzy extended information filtering for an AMR equipped with a 360° laser scanner with at least three retro-reflectors. If three reflectors are installed on the walls surrounding the workspace, the static position and orientation of the AMR with respect to a reference world frame can be determined uniquely by means of exactly measuring the bearings of the reflectors and the proposed three-point triangulation method. In order to reduce the sensitivity to measurement errors, more than three reflectors placed at appropriate positions are required; the static pose estimation errors can be significantly reduced via the FEIF-based sensor fusion method. With the same configuration of the laser scanner and the reflectors, the proposed posture tracking method has been shown capable of continuously keeping trace of the pose of the robot navigating on a planned path at slow speeds. Through simulations and experimental results, the proposed methods have been proven to not only reduce the accumulation errors due to the dead-reckoning method, but also provide more accurate posture estimation and tracking. Moreover, the developed method can be extensively applied to localize mobile robots in various occasions and tasks.

Acknowledgment The authors gratefully acknowledge financial support from the National Science Council of the Republic of China under Grant NSC 93-2213-E-005-049.

References

1. Abdelnour, G., Chand, S., Chiu, S., Kido, T.: On-line detection & correction of Kalman filter divergence by fuzzy logic. Proceeding of the American Control Conference, pp. 1835–1839 (1993)

2. Angelov, P., Filev, D.: An approach to on-line identification of Takagi–Sugeno fuzzy models. IEEE Trans. Syst. Man Cybern. Part B. **34**(1), 484–498 (2004)
3. Borenstein, J., Everett, H.R., Feng, L.: Navigating Mobile Robots: Systems and Techniques. Wellesley, MA., AK Peters (1996)
4. Chang, C.F., Tsai, C.C., Hsu, J.C., Lin, S.C., Lin, C.C.: Laser self-localization for a mobile robot using retro-reflector landmarks. Proceedings of American Control Conference, Denver, Colorado USA, pp. 2471–2476 (2003)
5. Decker, S., Gander, H., Vincze, M., Prenninger, J.P.: Dynamic measurement of position and orientation of robots. IEEE Trans. Instrum. Meas. **41**(6), 897–901 (1992)
6. Dubrawski, A., Siemiatkowska, B.: A method for tracking pose of a mobile robot equipped with a scanning laser range finder. Proceeding of the IEEE International Conference on Robotics and Automation, Belgium, pp. 2518–2523 (1998)
7. Forsberg, J., Larsson U., Wernersson, Åke.: Mobile robot navigation using the range-weighted Hough transform. IEEE Robotics and Automation Magazine pp. 18–26 (1995)
8. Jensfelt, P., Kristensen, S.: Active global localization for a mobile robot using multiple hypothesis tracking. IEEE Trans. Robot. Autom. **17**(5), 748–760 (2001)
9. Kim, Y.H.: Localization of a mobile robot using a laser range finder in a hierarchical navigation system. IEEE Proceedings of Southeastcon, pp. 712–720 (1993)
10. Kobayashi, K., Cheok, K.C., Watanabe, K., Munekata, F.: Accurate differential global positioning system via fuzzy logic Kalman filter sensor fusion technique. IEEE Trans. Ind. Electron. **45**, (3), 510–518 (1998)
11. McGillem, C.D., Rappaport, T.S.: Infra-red location system for navigation of autonomous vehicles. Proceedings of IEEE International Conference on Robotics and Automation, pp. 1236–1238 (1998)
12. Mutambara, A.G.O.: ecentralized Estimation and Control for Multisensor Systems, CRC (1998)
13. Nishizawa, T., Ohya, A., Yuta, S.: An implementation of on-board position estimation for a mobile robot. Proceeding of the IEEE International Conference on Robotics and Automation, pp. 395–400 (1995)
14. Rupp, T., Levi, P.: Optimized Landmark Arrangement for Absolute Localization. – A Practical Approach. Proceedings of IEEE/RSJ International Conference on Intelligent Robots and System, pp. 448–453 (2000)
15. Sasiadek, J.Z., Wang, Q.: Sensor fusion based on fuzzy Kalman filtering for autonomous robot vehicle. Proceeding of the IEEE Conference on Robotics and Automation, Detroit, Michigan, pp. 2970–2975 (1999)
16. Sasiadek, J.Z, Wang, Q., Zeremba, M.B.: Fuzzy adaptive Kalman filtering for INS/GPS data fusion. Proceedings of the 15th IEEE International Symposium on Intelligent Control, Rio, Patras, Greece, pp. 181–186 (2000)
17. Tsai, C.C., Hsu, J.C., Chang, C.F., Lin, S.C., Lin, C.C.: Laser self-localization for a mobile robot using retro-reflector landmarks. Proceeding of International Conference on Automation Technology, Taiwan, R. O. C., pp. 521–526 (2003)
18. Tsai, C.C., Lin, H.H., Hsu, J.C.: Fuzzy Adaptive extended information filtering. Int. J. Fuzzy Syst. **7**(1), 31–39 (2005)
19. Tsumura, T., Okubo, H., Komatsu, N.: A 3-D position and attitude measurement system using laser scanners and corner cubes. Proceeding of IEEE/RSJ International Conference on Intelligent Robots and System, Japan, pp. 604–609 (1993)
20. Jensfelt, P., Christensen, H.I.: Pose tracking using laser scanning and minimalistic environmental models. IEEE Trans. Robot. Autom. **17**(2), 138–147 (2001)
21. Toshihiro, N., Akihisa, O., Shin'ichi, Y.: An implementation of on-board position estimation for a mobile robot—EKF-based odometry and laser reflector landmarks detection. Proceedings of IEEE International Conference on Robotics and Automation, pp. 395–400 (1995)